Supplementary Information (SI) for Journal of Materials Chemistry C.

The importance of accounting for non-radiative decay when screening materials for singlet fission: the case of Pigment Red 254
Supplementary Information

Daniel Hook[1,5], Rachel Kilbride[2], Daniel J. Gillard[1], Samara Medina Rivero[1,3], Ravi Kumar Venkatraman[1,4], James P. Pidgeon[1], Alexander Tartakovskii[1,7], and Jenny Clark[1,6]

[1] Department of Physics and Astronomy, University of Sheffield, S3 7RH, UK
[2] Department of Chemistry, University of Sheffield, Sheffield, S3 7HF, UK
[3] Department of Physical Chemistry, University of Málaga Andalucia-Tech Campus de Teatinos s/n, 29071 Málaga (Spain)
[4] Department of Chemistry, SRM Institute of Science and Technology, Kattankulathur, Chengalpattu - 603 203, Tamil Nadu, India
[5] `danhook42@outlook.com`
[6] `jenny.clark@sheffield.ac.uk`
[7] `a.tartakovskii@sheffield.ac.uk`

Table S1. Table of sample temperature as set by water bath heater versus measured temperature of substrate back surface.

Set temperature (°C)	Measured temperature (°C)
25	23
35	29.5
45	35
50	38
55	40
65	44

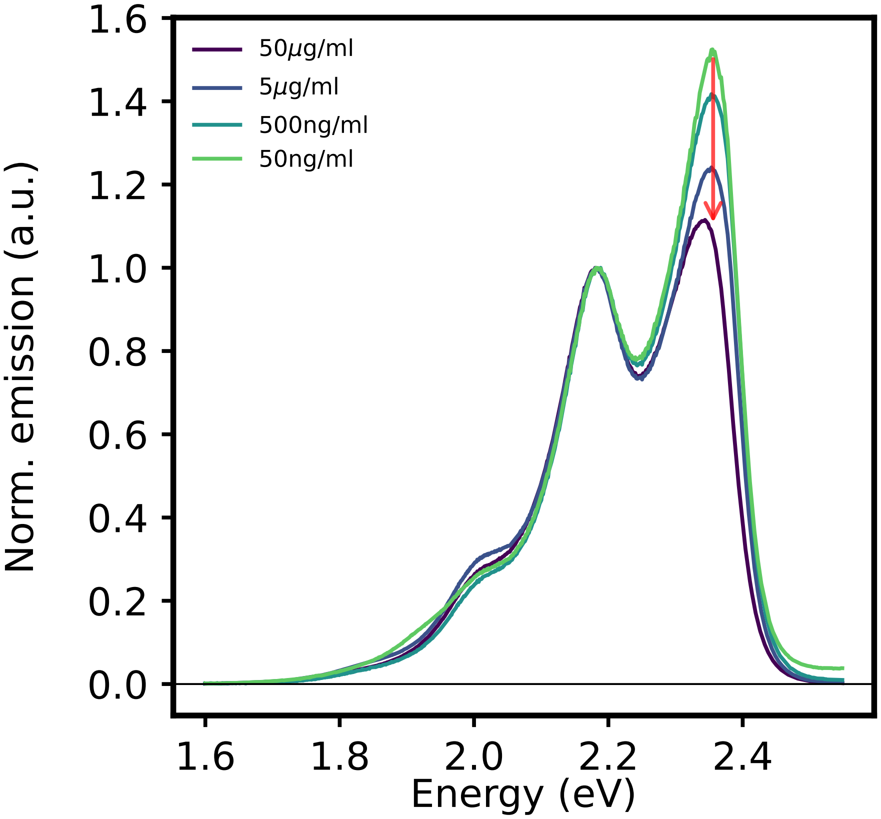

Fig. S1. Concentration dependent emission spectra of Red254 in solution of DMSO. These spectra are normalised to their second vibrational peak, to demonstrate any potential loss of emission due to self absorption in the primary peak, or through aggregate effects. The loss of emission at higher energies can be explained through either of these effects, but its persistence over multiple orders of magnitude of concentration suggests self-absorption effects. However, at 50 μg/ml, this reduction also shifts the maximum of the emission to lower energy. Between 500 ng/ml and 50 ng/ml there is no such shift. As such, 50 ng/ml was used as the concentration for analysis of the solution emission spectrum, as it is at this concentration that we can be most confident that the solution sample does not show aggregate effects.

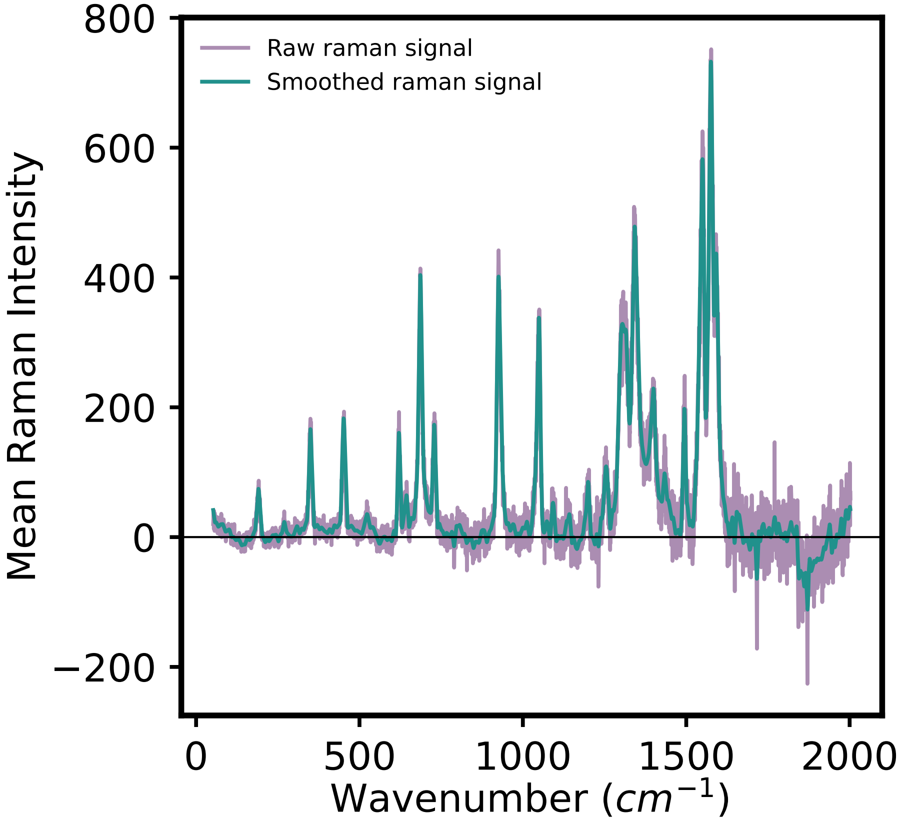

Fig. S2. Resonance raman spectrum of a thin film sample of Red254 on a quartz substrate. This spectrum was used to identify raman modes for the Franck-Condon fitting of the Red254 steady state solution spectra, as shown in figs. S3, S4. The raman spectrum shown (”raw” raman signal, purple.) was filtered via a low-pass fourier filter to remove high-frequency noise and make the underlying raman spectrum clearer, shown as the ”filtered” raman signal, in green.

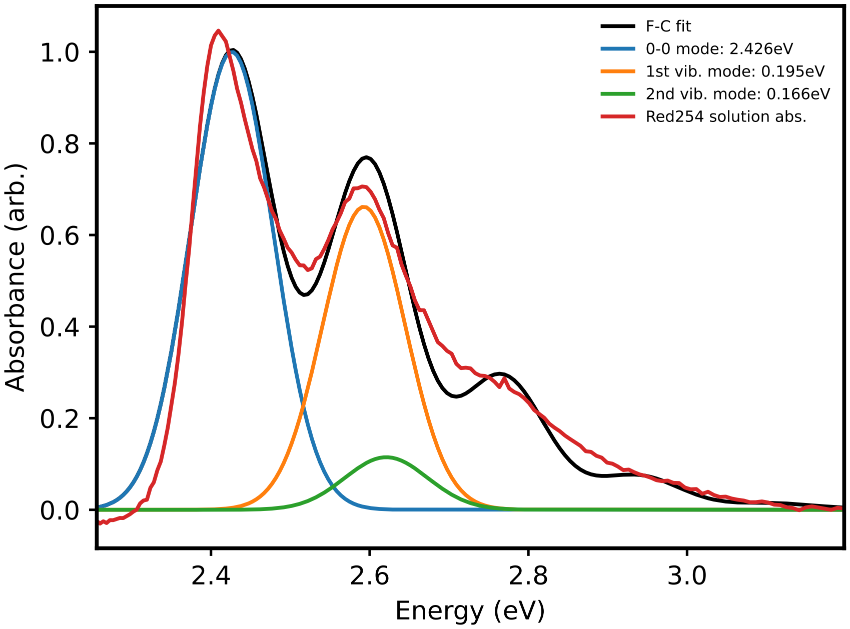

Fig. S3. Franck-Condon fit to the Red254 in DMSO solution-phase absorption spectrum, with the vibrational energies obtained from resonance Raman spectroscopy. The vibrational peaks are shown here to better demonstrate the fit

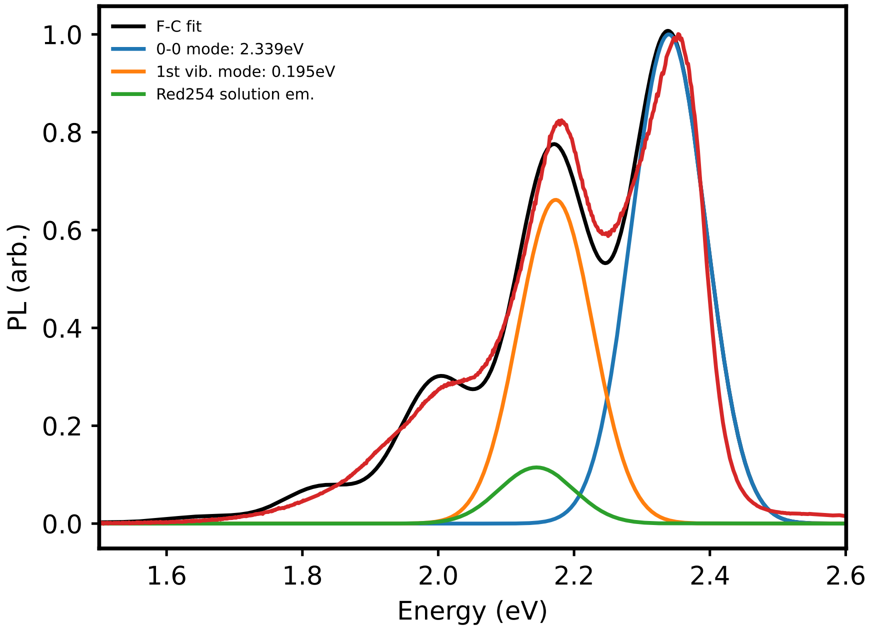

Fig. S4. Franck-Condon fit to the Red254 in DMSO solution-phase emission spectrum, with the vibrational energies obtained from resonance Raman spectroscopy, and the Huang-Rhys parameters taken from the absorption spectrum fit. The vibrational peaks are shown here to better demonstrate the fit.

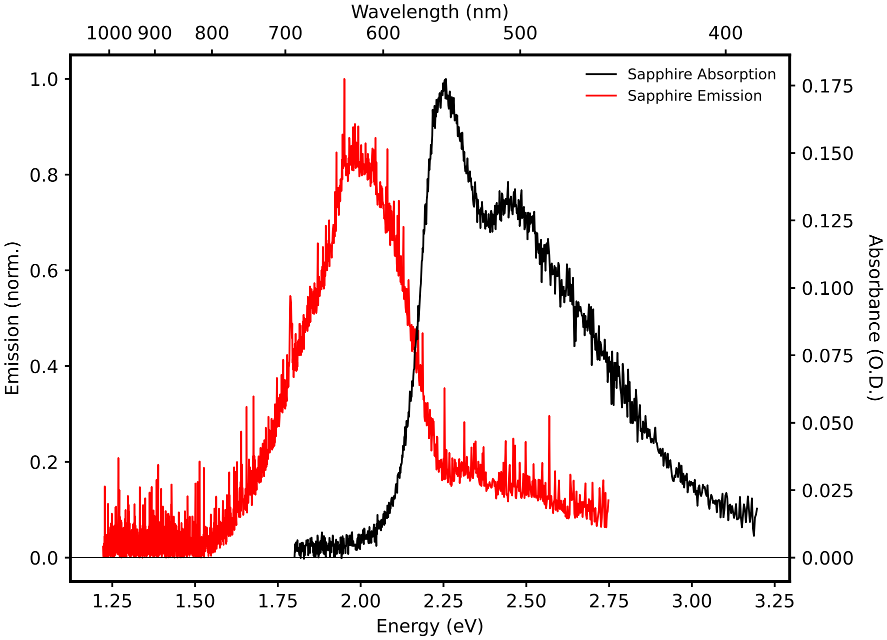

Fig. S5. Steady state UV-vis absorption and emission spectra of thin films of Red254 on sapphire substrates.

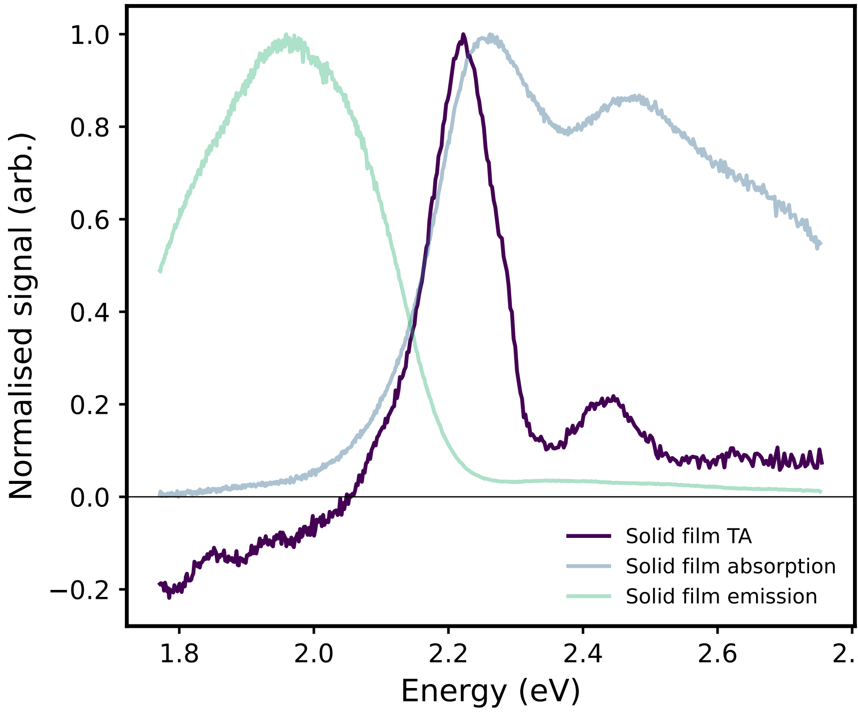

Fig. S6. Comparison of transient absorption spectrum with steady state absorption and emission spectra of a thin film of Red254, illustrating the motivation behind assigning each region of the TA spectrum to each feature. The large positive signal and secondary positive peak overlap with the steady-state absorption, motivating it's assignment to the ground state bleach feature. The GSB has very different structure compared to the steady state spectrum, with the primary 0-0 peak being proportionally much higher than expected. This combined with no visible stimulated emission suggests there is significant photo-induced absorption overlaid with these features, resulting in the increased absorption below ∼2.1 eV

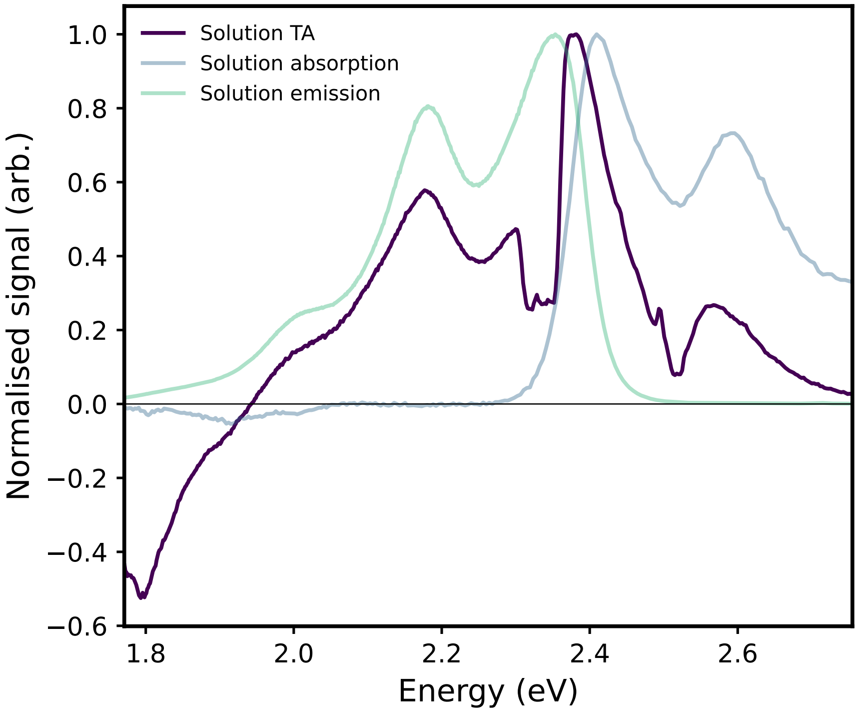

Fig. S7. Comparison of transient absorption spectrum with steady state absorption and emission spectra of a dilute solution of Red254 in DMSO, illustrating the motivation behind assigning each region of the TA spectrum to each feature. The broad positive feature above ∼1.9 eV matches well to the structure of the steady state absorption and emission spectra, with the region above ∼2.4 eV matching well to the absorption spectrum, and the remainder of the spectrum matching the emission spectrum. The remaining negative signal below ∼1.9 eV is then naively assigned to photoinduced absorption to higher singlet states.

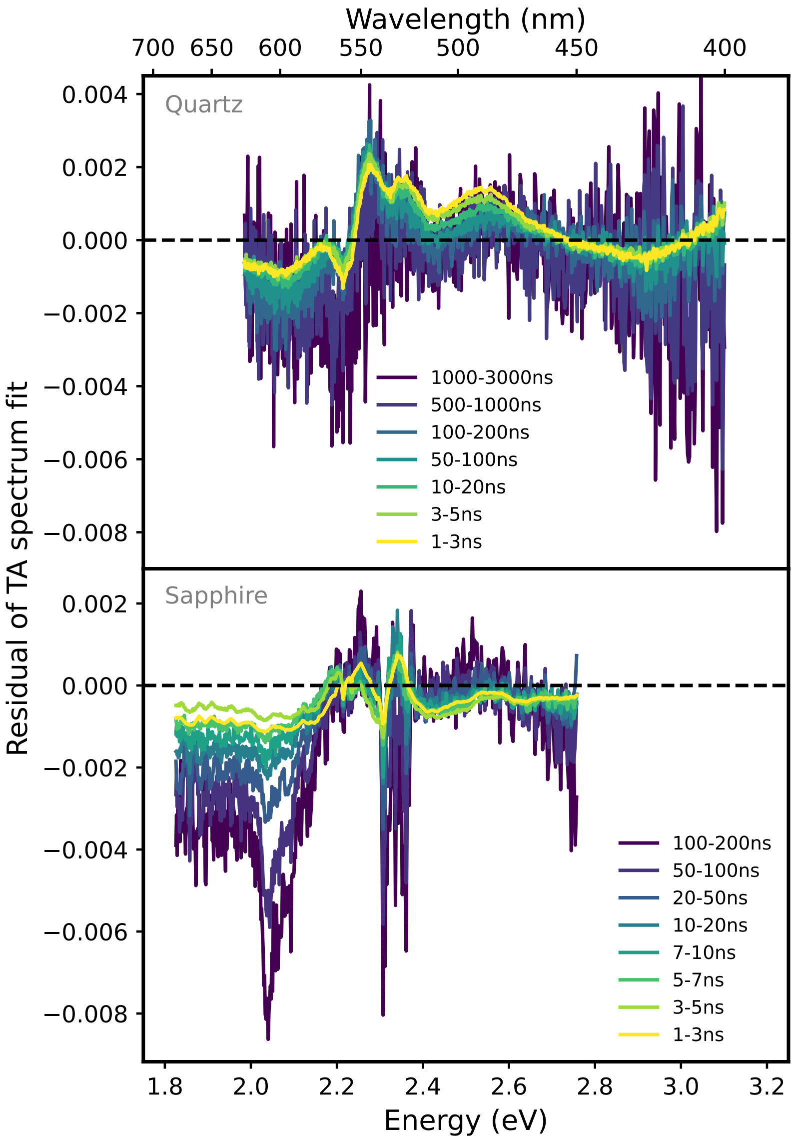

Fig. S8. Plot of residual error from a linear fit of the temperature dependent absorption spectra shown in fig. **??** to the long-time TA spectra at various time slices for thin films of Red254 on a quartz substrate (top) and on a sapphire substrate (bottom). This is done to ascertain if there are any time-dependent features obscured by the heat-based artefact that dominates the long-time TA spectrum. However, the noise of the resultant residual spectra makes positive identification difficult. The only time dependent feature in the residual spectra is observed at ∼2.05 eV in the sapphire spectra, which shows a photo-induced absorption feature increasing in magnitude after ∼10 ns, indicating the presence of a long-lived species in the solid film of Red254. However, this is not conclusive as a similar feature is not observed in the quartz data. The vertical blue line indicates the pump wavelength for the TA data.

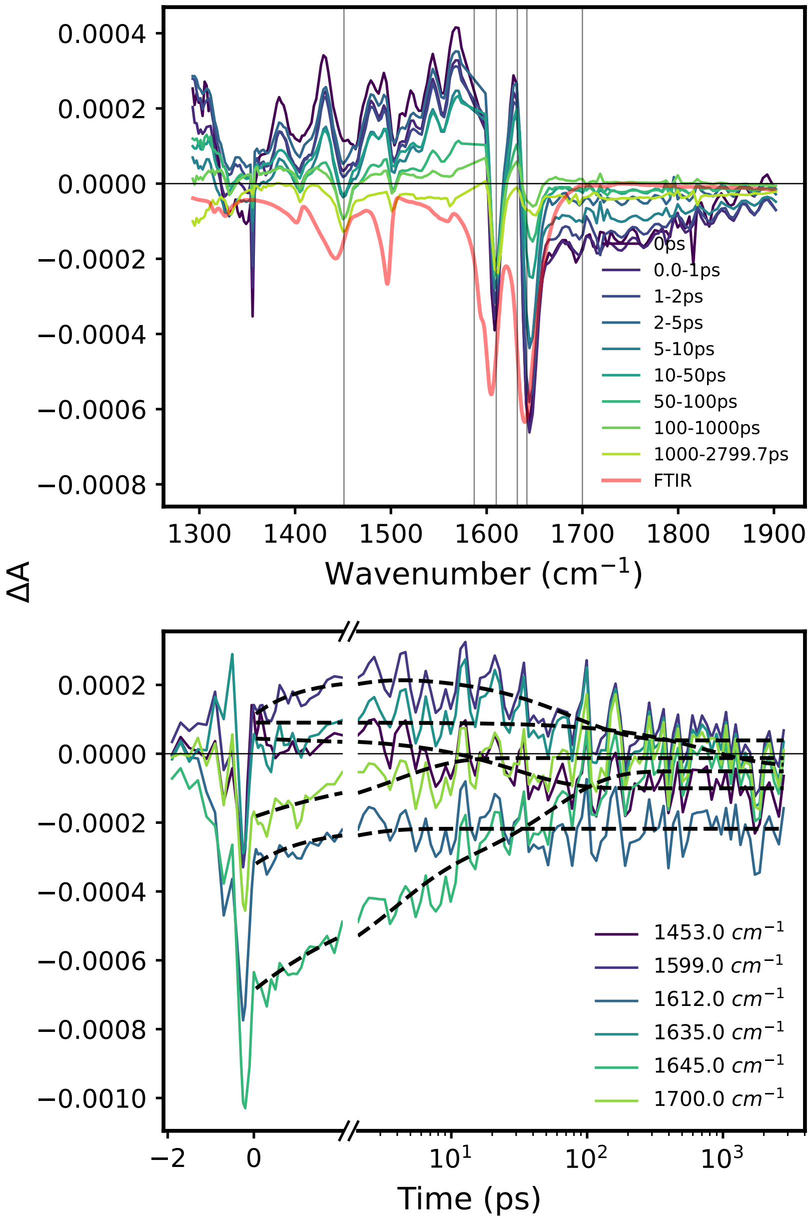

Fig. S9. Time Resolved Infra-Red (TRIR) spectra (top) and kinetics (bottom) of thin film of Red254 on calcium fluoride window substrate, using a pump wavelength of 520 nm and power of 0.5 mW. An additional broad electronic signal was seen in all TRIR spectra, and was subtracted from the overall spectrum by subtracting the signal between 2000-2100 cm^{-1}, as the signal appeared the same across the entire spectrum. The subtracted kinetics are shown in figure **??**. Overlaid with these spectra is the inverted Fourier Transform Infra-Red (FTIR) obtained from the RAL spectrometer, to assist in identifying the peaks. The locations of the kinetic slices used in the TRIR kinetics (bottom) are marked by grey lines on the figure. Exponential and bi-exponential fits to the data are shown on this graph as dotted black lines.

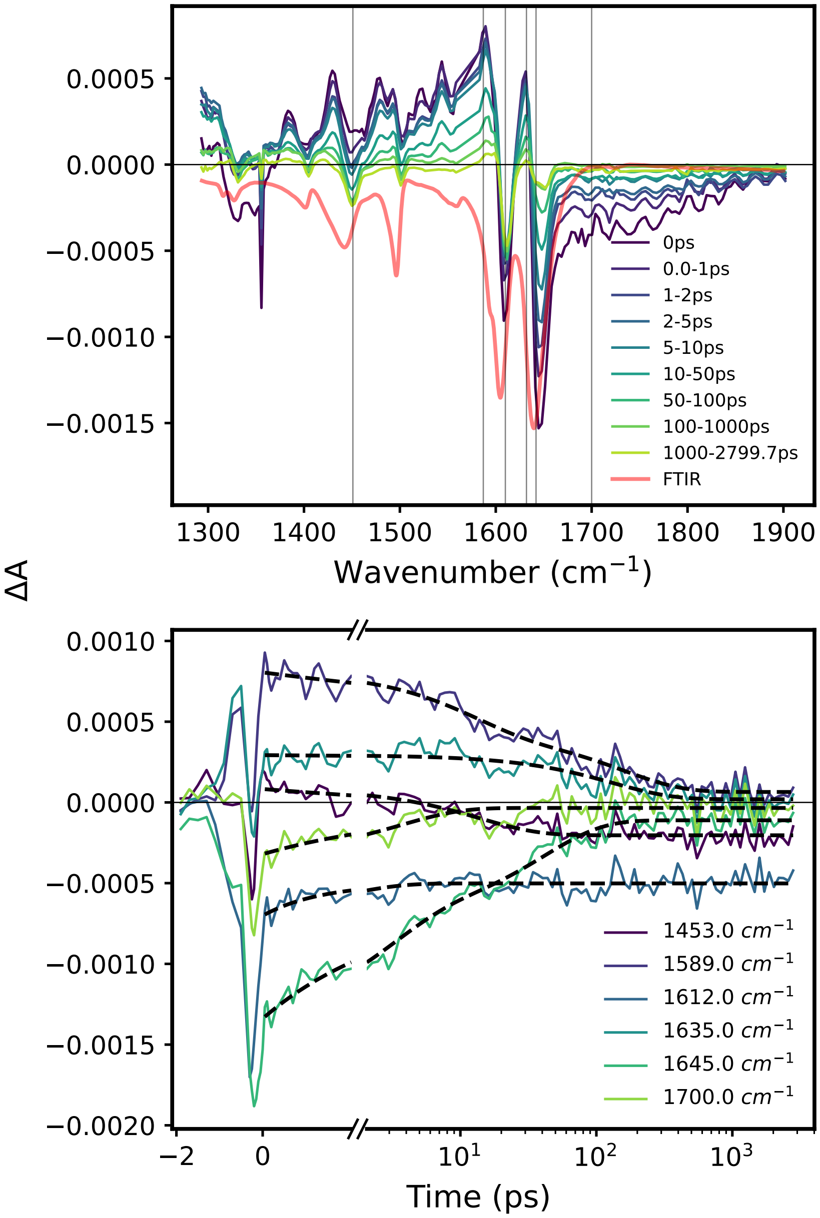

Fig. S10. Time Resolved Infra-Red (TRIR) spectra (top) and kinetics (bottom) of thin film of Red254 on calcium fluoride window substrate, using a pump wavelength of 520 nm and power of 1 mW. An additional broad electronic signal was seen in all TRIR spectra, and was subtracted from the overall spectrum by subtracting the signal between 2000-2100 cm^{-1}, as the signal appeared the same across the entire spectrum. The subtracted kinetics are shown in figure **??**. Overlaid with these spectra is the inverted Fourier Transform Infra-Red (FTIR) obtained from the RAL spectrometer, to assist in identifying the peaks. The locations of the kinetic slices used in the TRIR kinetics (bottom) are marked by grey lines on the figure. Exponential and bi-exponential fits to the data are shown on this graph as dotted black lines.

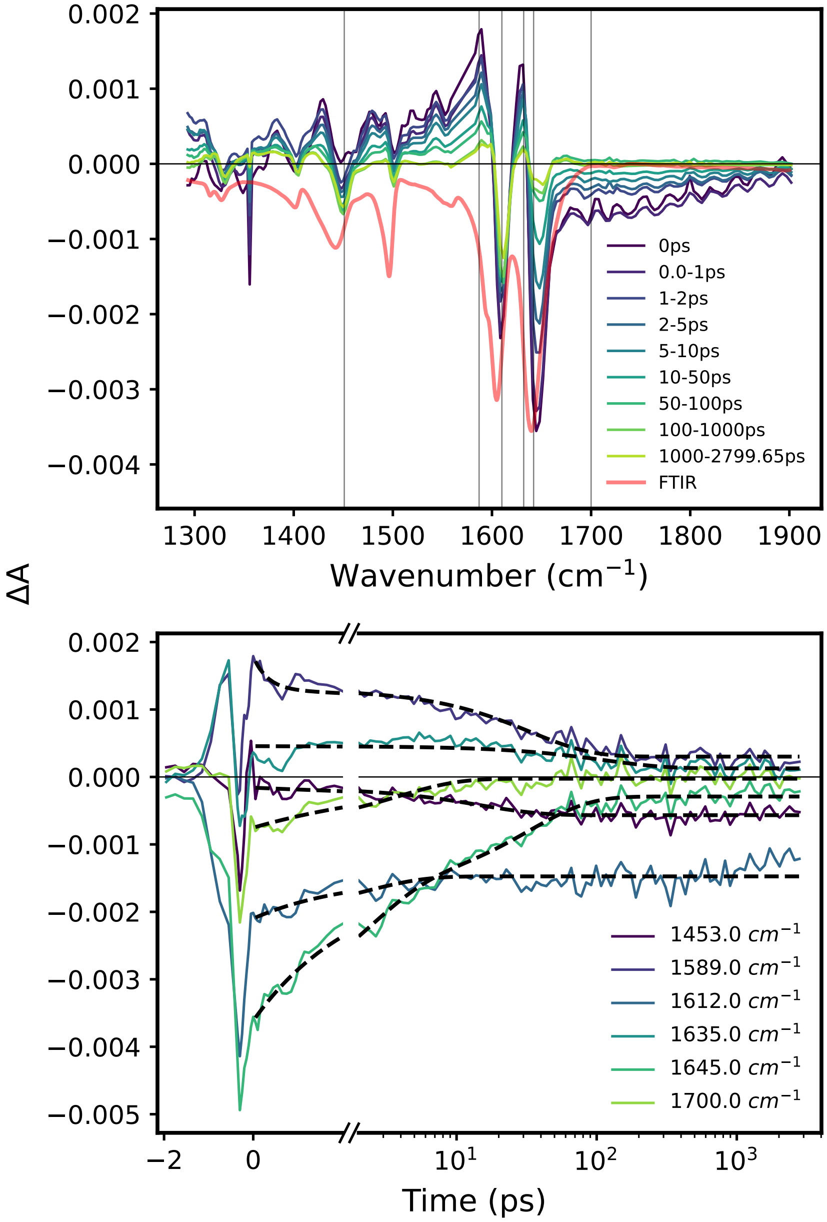

Fig. S11. Time Resolved Infra-Red (TRIR) spectra (top) and kinetics (bottom) of thin film of Red254 on calcium fluoride window substrate, using a pump wavelength of 520 nm and power of 2.5 mW. An additional broad electronic signal was seen in all TRIR spectra, and was subtracted from the overall spectrum by subtracting the signal between 2000-2100 cm^{-1}, as the signal appeared the same across the entire spectrum. The subtracted kinetics are shown in figure **??**. Overlaid with these spectra is the inverted Fourier Transform Infra-Red (FTIR) obtained from the RAL spectrometer, to assist in identifying the peaks. The locations of the kinetic slices used in the TRIR kinetics (bottom) are marked by grey lines on the figure. Exponential and bi-exponential fits to the data are shown on this graph as dotted black lines.

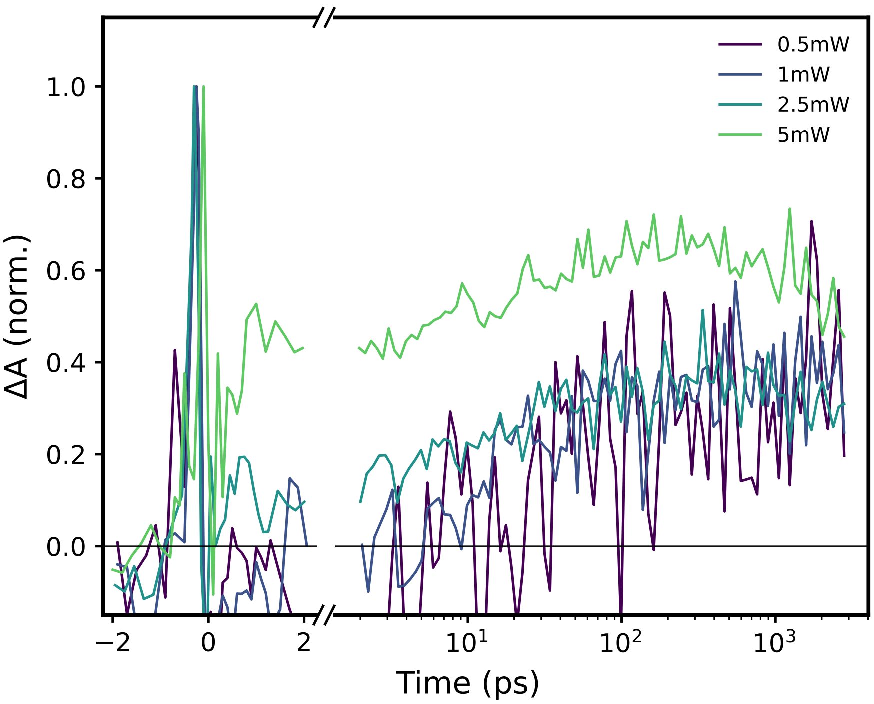

Fig. S12. Normalised kinetic decays of the 1451 cm^{-1} kinetic slice of time-resolved infra-red spectrum of Red254 evaporated thin film on calcium fluoride substrate, using an excitation wavelength of 520 nm at fluences of 0.5 mW, 1 mW, 2.5 mW, and 5 mW. There is some variation in the 2.5 mW and 5 mW fluence plots, with the 5 mW decay being significantly more intense at early times. This may correspond to an increase in un-subtracted electronic signal remaining in the lower end of the spectrum.

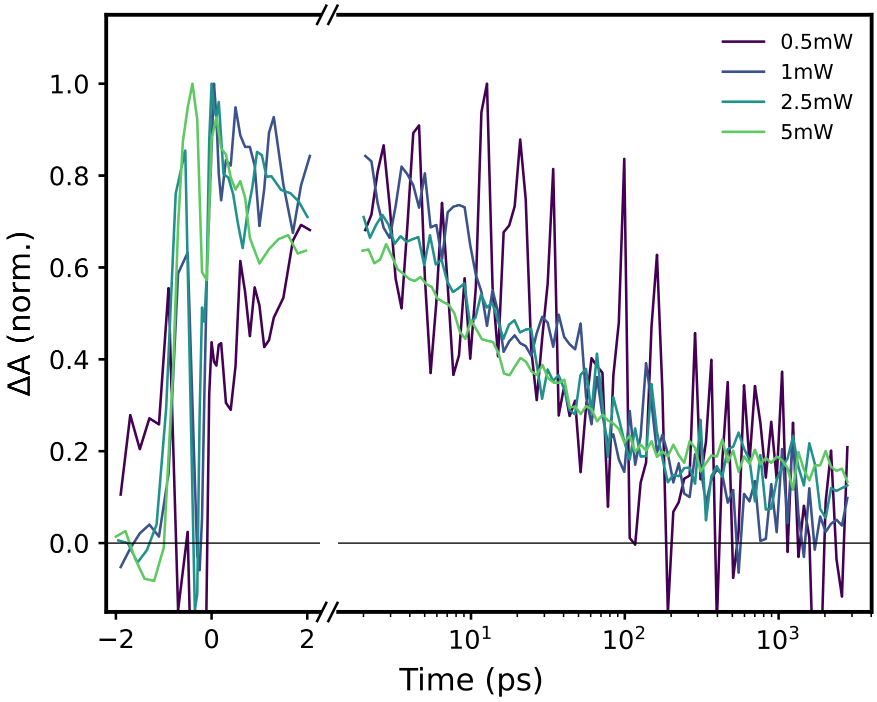

Fig. S13. Normalised kinetic decays of the 1589 cm^{-1} kinetic slice of time-resolved infra-red spectrum of Red254 evaporated thin film on calcium fluoride substrate, using an excitation wavelength of 520 nm at fluences of 0.5 mW, 1 mW, 2.5 mW, and 5 mW. Very little variation is visible in the kinetic lineshape, except for the 0.5 mW fluence, which shows higher noise than the others and has a different shape at early times.

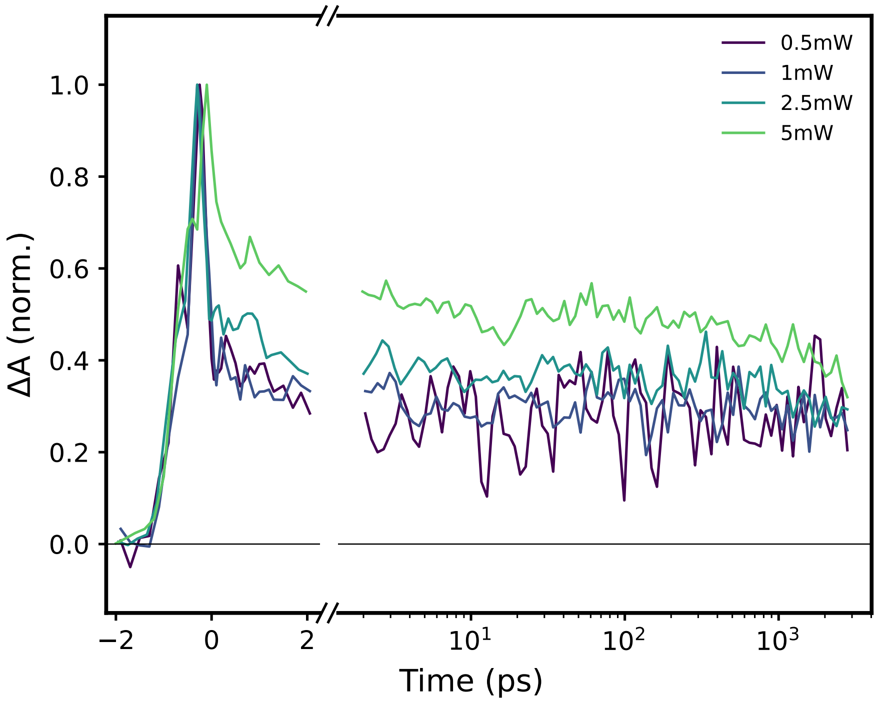

Fig. S14. Normalised kinetic decays of the 1610 cm^{-1} kinetic slice of time-resolved infra-red spectrum of Red254 evaporated thin film on calcium fluoride substrate, using an excitation wavelength of 520 nm at fluences of 0.5 mW, 1 mW, 2.5 mW, and 5 mW. The 0.5 mW kinetic is shows some additional noise, and the 5 mW kinetic shows some additional signal at early times.

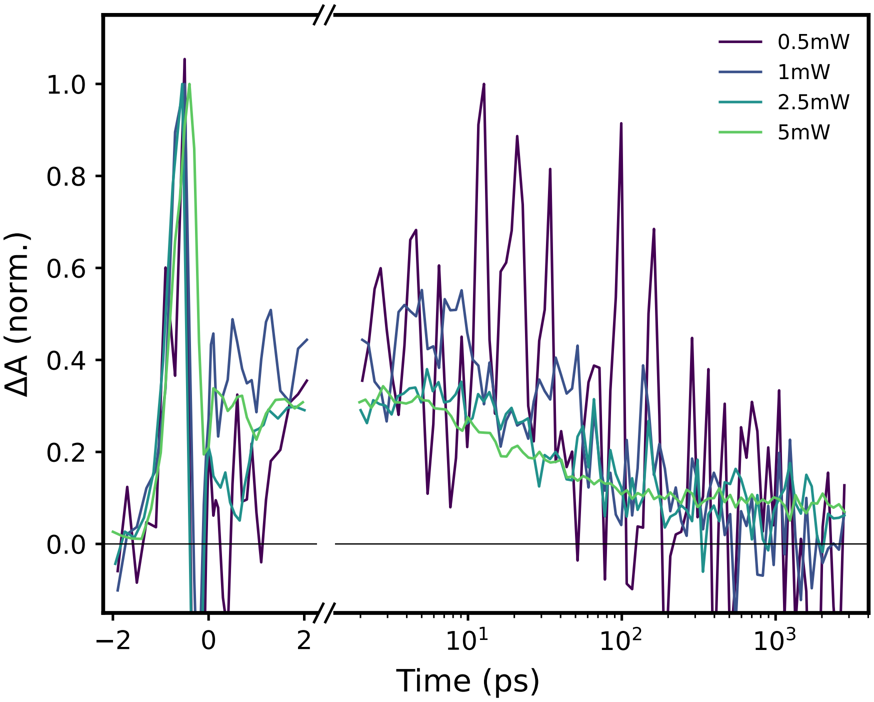

Fig. S15. Normalised kinetic decays of the 1627 cm^{-1} kinetic slice of time-resolved infra-red spectrum of Red254 evaporated thin film on calcium fluoride substrate, using an excitation wavelength of 520 nm at fluences of 0.5 mW, 1 mW, 2.5 mW, and 5 mW. While there is little visible variation form this plot, the 0.5 mW kinetic is highly noisy.

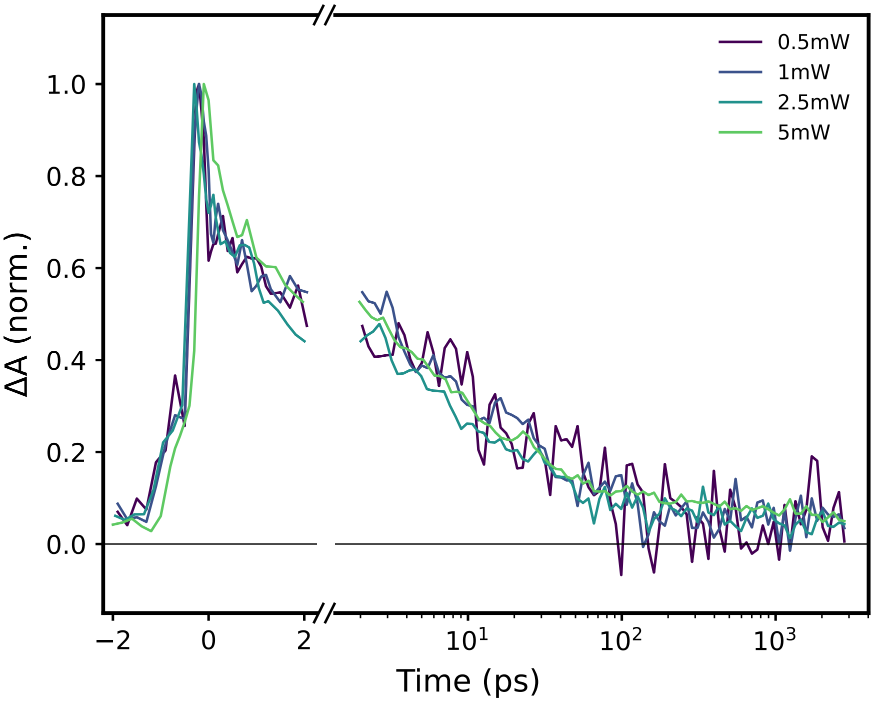

Fig. S16. Normalised kinetic decays of the 1643 cm^{-1} kinetic slice of time-resolved infra-red spectrum of Red254 evaporated thin film on calcium fluoride substrate, using an excitation wavelength of 520 nm at fluences of 0.5 mW, 1 mW, 2.5 mW, and 5 mW.

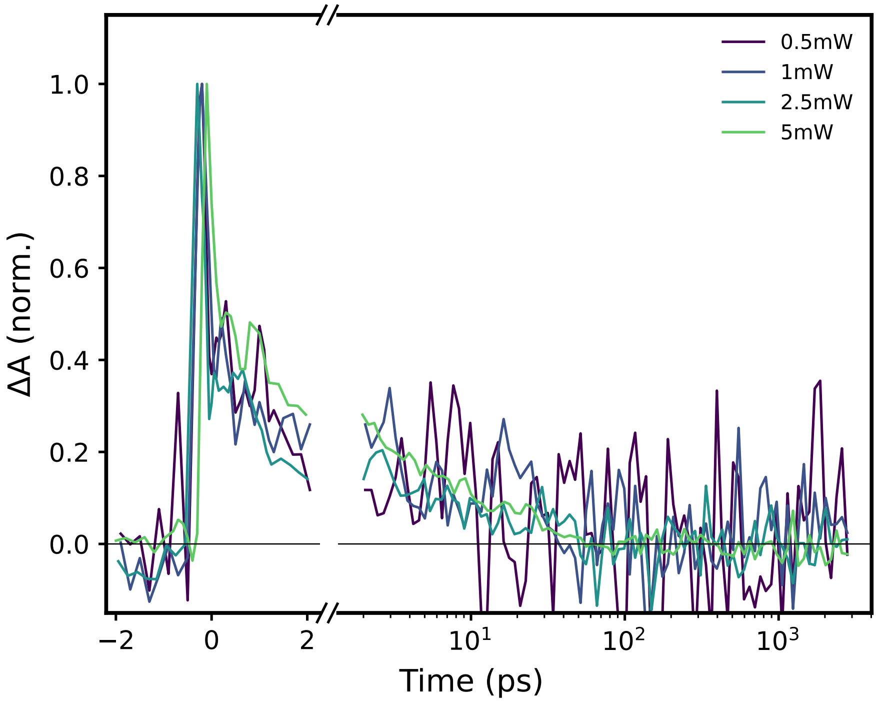

Fig. S17. Normalised kinetic decays of the 1703 cm^{-1} kinetic slice of time-resolved infra-red spectrum of Red254 evaporated thin film on calcium fluoride substrate, using an excitation wavelength of 520 nm at fluences of 0.5 mW, 1 mW, 2.5 mW, and 5 mW. There is significant noise in the 0.5 mW kinetic

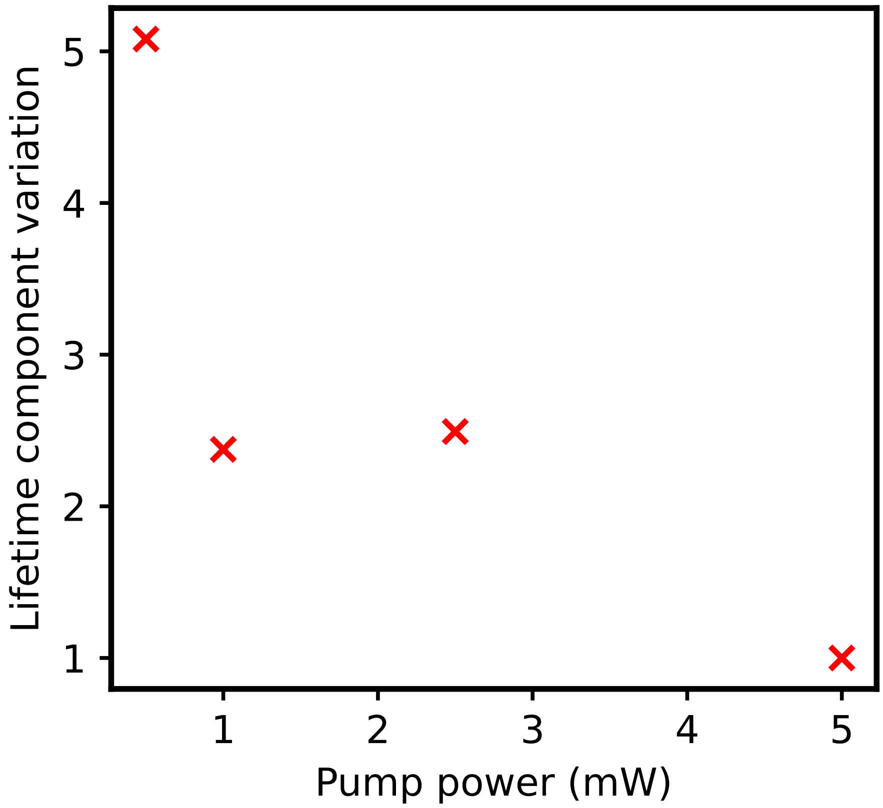

Fig. S18. Fluence dependence of fitted exponential lifetimes to the 1451 cm^{-1} kinetic slice of the TRIR spectra of Red254 on calcium fluoride substrate, normalised to the 5 mW kinetic. Lifetimes show large variations, especially at the extremal fluences, with the 0.5 mW kinetic having a lifetime 5 times as long as the 5 mW kinetic. However, this variation can be partially explained due to the large noise to signal ratio visible in this lowest power kinetic

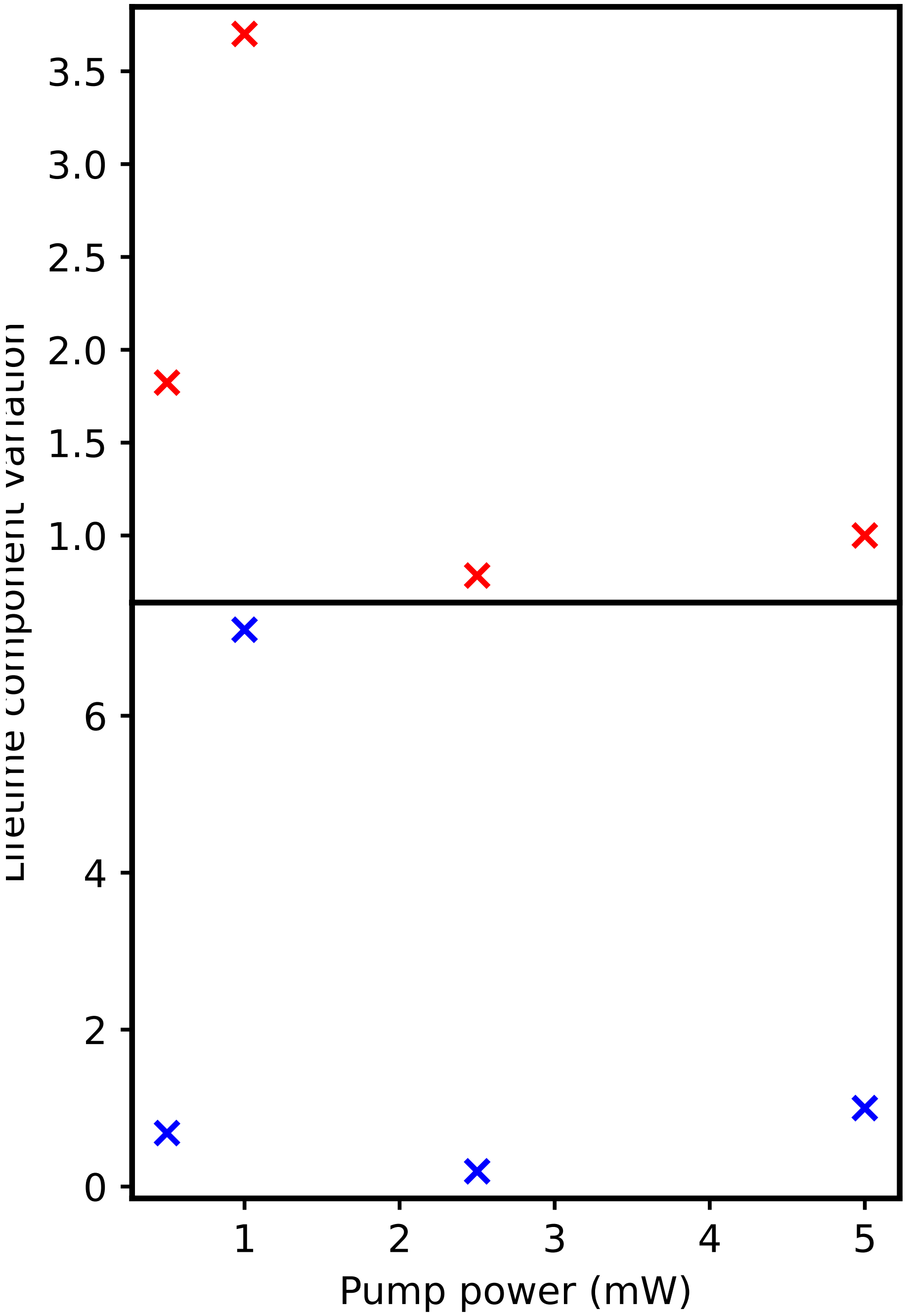

Fig. S19. Fluence dependence of fitted exponential lifetimes to the 1589 cm^{-1} kinetic slice of the TRIR spectra of Red254 on calcium fluoride substrate, normalised to the 5 mW kinetic. While there is some variation of lifetime with fluence, there is no monotonic fluence dependence. The 0.5 mW fluence lifetime is a standout from the rest, as the shape of the kinetic is different at this wavenumber, though this may be in part due to the high noise of this fluence kinetic. The lifetime of the 1 mW fluence kinetic is the highest, over 3.5 times that of the 5 mW kinetic, and there is little change between the 2.5 and 5 mW kinetic lifetimes.

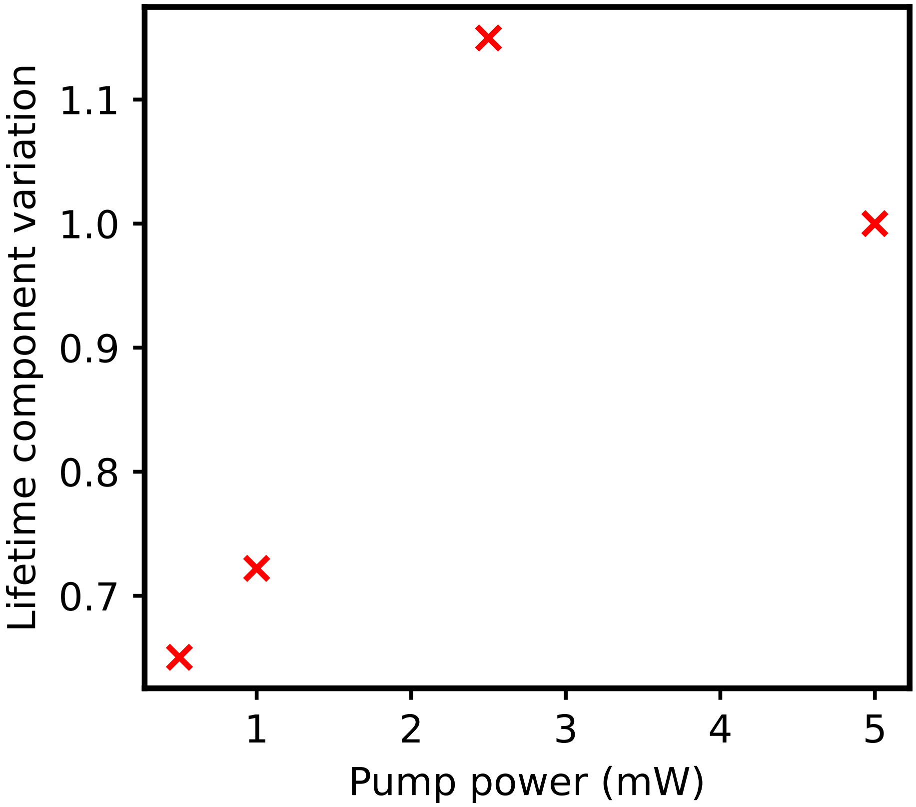

Fig. S20. Fluence dependence of fitted exponential lifetimes to the 1610 cm^{-1} kinetic slice of the TRIR spectra of Red254 on calcium fluoride substrate, normalised to the 5 mW kinetic. This kinetic shows a faster decay at lower fluence, indicating that a higher excitation concentration results in a longer lived population of this vibrational state

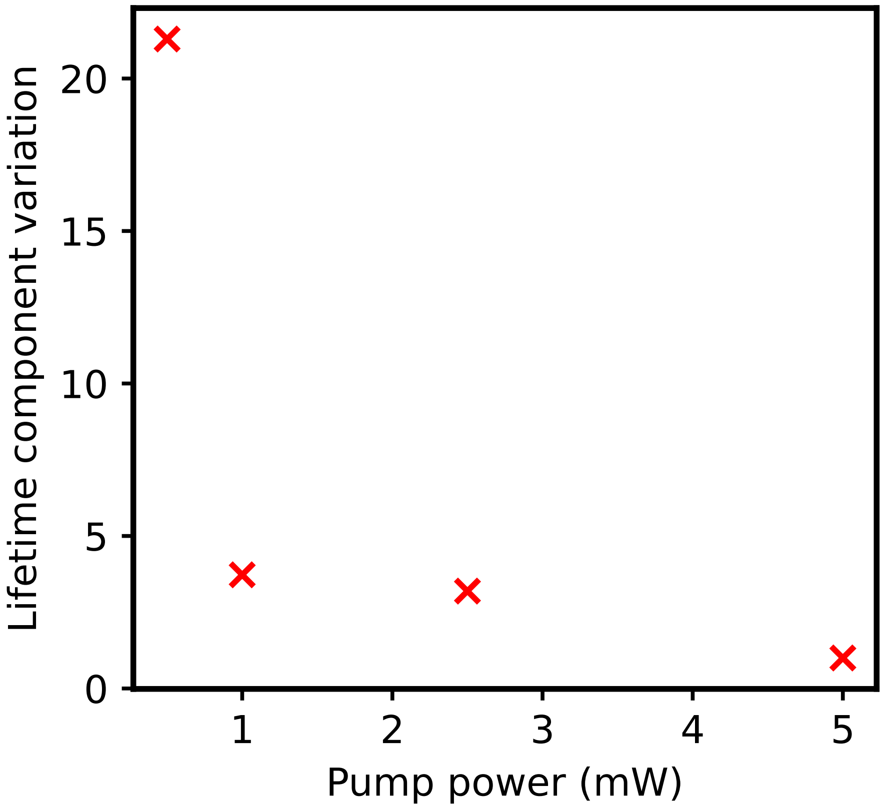

Fig. S21. Fluence dependence of fitted exponential lifetimes to the 1627 cm^{-1} kinetic slice of the TRIR spectra of Red254 on calcium fluoride substrate, normalised to the 5 mW kinetic. The 0.5 mW lifetime has a much longer lifetime than the higher fluence measurements, although we attribute this mostly to the higher noise. The remaining components vary up to 4x greater than the 5 mW kinetic lifetime, indicating a small fluence dependence to the lifetime.

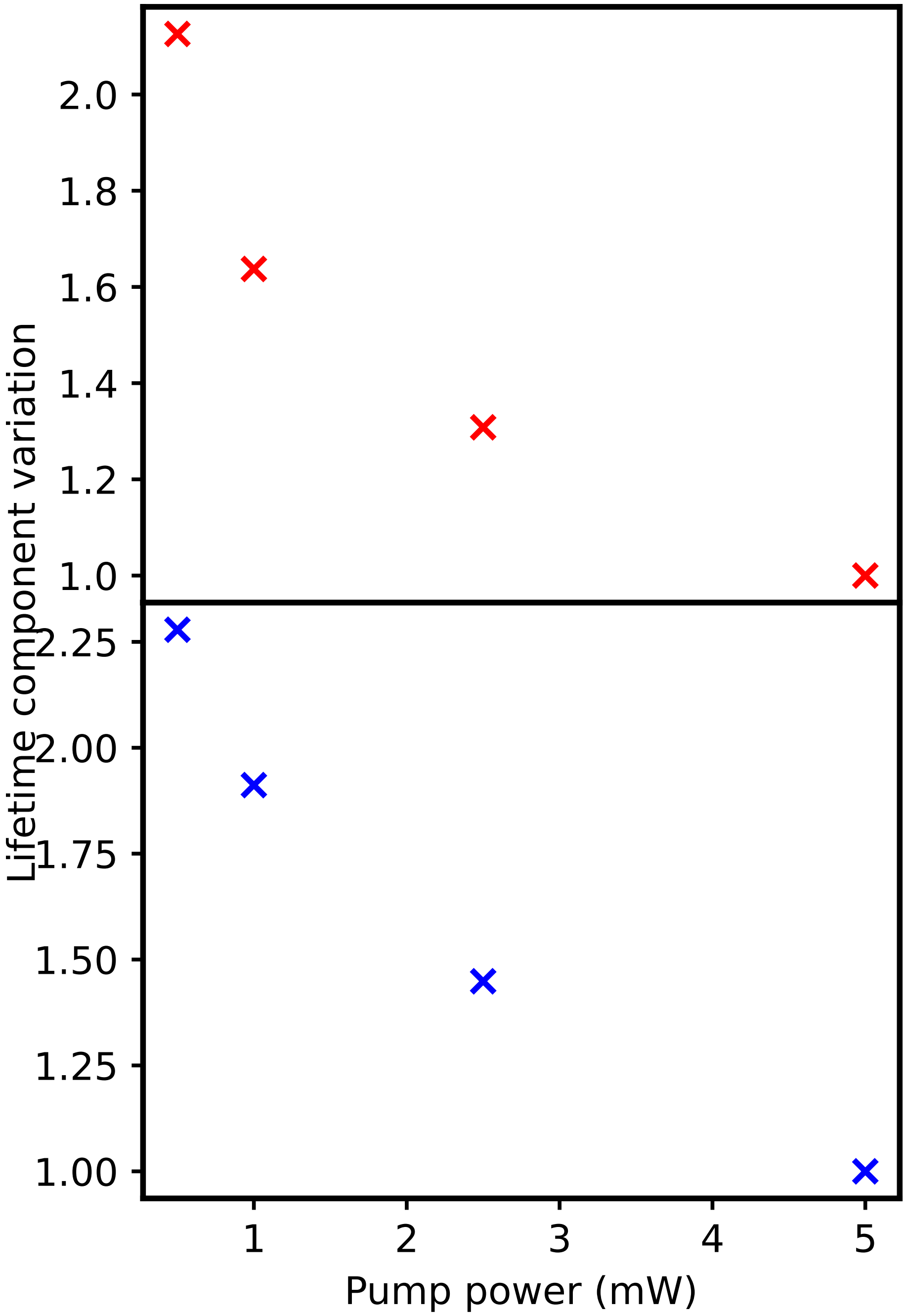

Fig. S22. Fluence dependence of the bi-exponential fit lifetimes of the 1643 cm^{-1} kinetic slice of the TRIR spectra of Red254 on calcium fluoride substrate, normalised to the 5 mW kinetic. In both cases, the lifetime components of these kinetics vary by ∼2 times, with a lower fluence resulting in a longer lifetime. This indicates an intermolecular component to the lifetime of this vibration, in that a higher excitation density results in a faster decay.

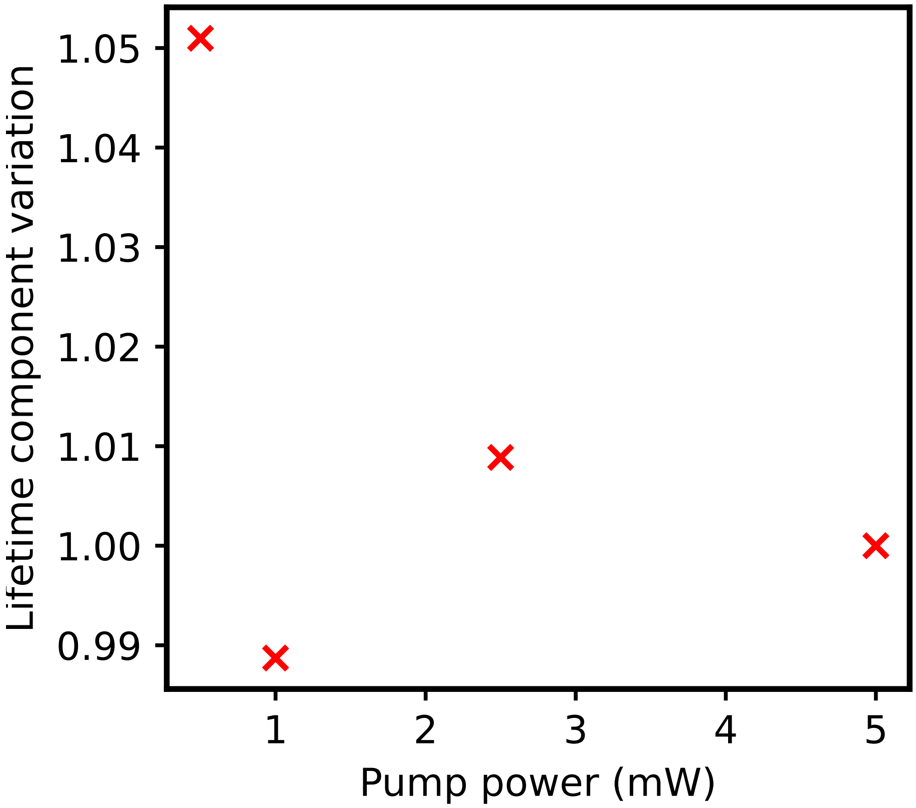

Fig. S23. Fluence dependence of fitted exponential lifetimes of the 1703 cm^{-1} kinetic slice of the TRIR spectra of Red254 on calcium fluoride substrate, normalised to the 5 mW kinetic. The lifetime only varies by ∼5% overall, indicating little to no fluence dependence of this kinetic

Table S2. Lifetimes of excited vibrational decays from Time-Resolved Infra-Red spectroscopy kinetics as shown in Figs. S9, S10 and S11

Wavenumber (cm^{-1})	τ_1 (ps)	τ_2 (ps)	$\delta\tau_1$ (ps)	$\delta\tau_2$ (ps)
0.5 mW				
1451	30	-	8.5	-
1589	1.1	78	0.8	24
1610	1.2	-	0.64	-
1627	800	-	530	-
1643	3.4	53	0.95	13.2
1703	3.9	-	1.3	-
1 mW				
1451	14	-	2.1	-
1589	12	160	2.85	39
1610	1.35	-	0.41	-
1627	130	-	26	-
1643	2.9	41	0.45	5.5
1703	3.7	-	0.78	-
2.5 mW				
1451	14.6	-	2.6	-
1589	0.32	33	0.11	3.1
1610	2.1	-	0.49	-
1627	110	-	34	-
1643	2.2	33	0.20	3.4
1703	3.8	-	0.48	-